Journal of Physics: Conference Series **228** (2010) 012044 doi:10.1088/1742-6596/228/1/012044

Arm locking with Doppler estimation errors

Yinan Yu, Vinzenz Wand, Shawn Mitryk, Guido Mueller

Department of Physics, University of Florida, Gainesville, FL 32611, USA

E-mail: yinan@phys.ufl.edu

Abstract. At the University of Florida we developed the University of Florida LISA Interferometer Simulator (UFLIS) in order to study LISA interferometry with hardware in the loop at a system level. One of the proposed laser frequency stabilization techniques in LISA is arm locking. Arm locking uses an adequately filtered linear combination of the LISA arm signals as a frequency reference. We will report about experiments in which we demonstrated arm locking using UFLIS. During these experiments we also discovered a problem associated with the Doppler shift of the return beam. The initial arm locking publications assumed that this Doppler shift can perfectly be subtracted inside the phasemeter or adds an insignificant offset to the sensor signal. However, the remaining Doppler knowledge error will cause a constant change in the laser frequency if unaccounted for. Several ways to circumvent this problem have been identified. We performed detailed simulations and started preliminary experiments to verify the performance of the proposed new controller designs.

1. Introduction

The Laser Interferometer Space Antenna (LISA) is a joint NASA-ESA mission to detect gravitational waves in the frequency region of 3×10^{-5} Hz to 1 Hz by means of laser interferometry [1]. LISA synthesizes three spacecraft arranged in an equilateral triangle constellation with each arm length of 5×10^9 m to reach a strain sensitivity of $10^{-21}/\sqrt{\text{Hz}}$ at 3 mHz. A variety of laser frequency stabilization techniques need to be introduced to suppress the laser frequency/phase noise to achieve this sensitivity. The first step is to stabilize the laser frequency to a resonant optical cavity or other local frequency reference. The second step is arm locking, which uses the LISA arms as a stable reference [2, 3]. The last step is known as time delay interferometry (TDI). This is a data post-processing technique to synthesize individual interferometer outputs in order to suppress the laser frequency/phase noise and clock noise to reach the LISA requirement.

The University of Florida LISA Interferometer Simulator (UFLIS) [4] is a benchtop hardware simulator used to simulate LISA interferometry and gravitational wave detections under LISA-like conditions. It incorporates the light travel time as well as variable Doppler shifts in each interferometer arm using electronic phase delays (EPD) [5]. The EPD unit includes an IQ phasemeter which extracts the frequency fluctuations of the incoming signal and sends the frequency information to a memory buffer. At the memory buffer the frequency information is stored for a certain amount of time and then is sent to a numerically control oscillator (NCO) to regenerate a delayed copy of the original signal. During this routine, a Doppler frequency can be added to the nominal frequency of the original signal.

This feature allows us to experimentally study the Doppler induced frequency pulling effect in arm locking as well as proposed solutions to solve this problem. In this paper we will report

© 2010 IOP Publishing Ltd

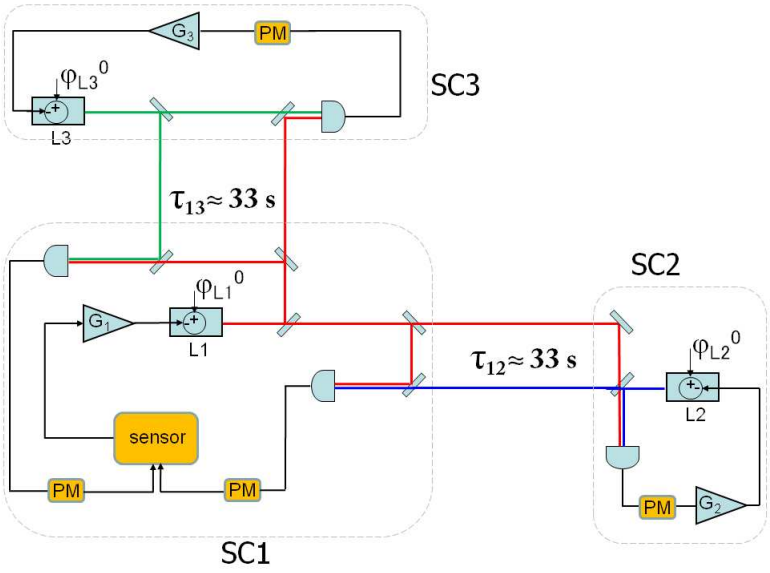

Figure 1. The baseline design of arm locking. The field from Laser 1 (L1) on the local SC1 is split and send to both far SC. The phase of the beat signals between L1 and the lasers L2 and L3 on SC2 and SC3 is measured with local phasemeter (PM) and used to phase lock L2 and L3 to L1. Similar beat signals are also measured on SC1 and used to generate the arm locking sensor signal.

on the current status of our arm locking experiments regarding the Doppler impact and on time-domain simulations of dual arm locking.

2. Arm Locking Architecture

2.1. Arm locking concepts

Figure 1 displays the baseline design for the discussed arm locking schemes. Among the three spacecraft (SC) of LISA, SC1 is used as the local or master spacecraft. The lasers on SC2 and SC3 are phase-locked to the incoming laser field of the laser from SC1. Therefore, once the laser fields from SC2 and SC3 are transmitted to SC1 and interfere with the local laser field, the phase of the interferometry signals is given by

$$S_{1i}(t) = \phi_1^0(t) - \phi_1^0(t - \tau_i), \quad i = 2, 3 \tag{1}$$

where $\phi_1^0(t)$ is the instantaneous phase of the pre-stabilized laser on SC1 and $\tau_i = \tau_{1i} + \tau_{i1} \approx$ 33s is the round trip time between SC1 and SC2/3. This relation assumes that all other noise sources such as the phase-locked loop error, clock noise and shot noise as well as the phase modulations from gravitational waves are negligible. These noise sources will limit the performance of arm locking but are not essential for the here discussed effects.

In the Laplace domain, we can derive the transfer function of the two LISA arms from the interferometer outputs described above:

$$P_{1i}(s) = \frac{\widetilde{S}_{1i}(s)}{\widetilde{\phi}_1^0(s)} = 1 - e^{-s\tau_i}, \quad i = 2, 3 \tag{2}$$

where $s = \sigma + i\omega$ is the Laplace variable. Then the two interferometer outputs are manipulated to construct an arm locking error signal. This process is described by a 2×1 mapping vector

S_k [6, 7]. Then the sensor transfer function will take the form

$$H_k(s) = P(s) \cdot S_k, \tag{3}$$

where

$$P(s) = \begin{bmatrix} P_{12}(s) \\ P_{13}(s) \end{bmatrix} \tag{4}$$

The specific form of the mapping vector S_k determines what arm locking scheme is utilized.

2.1.1. Single arm locking The simplest form of arm locking uses only one arm, $S_1 = [1, 0]$, to generate the error signal. For single arm locking the sensor transfer function simply takes the form

$$H_1(s) = P_{12} = 1 - e^{-s\tau_2}. \tag{5}$$

The delay term in the sensor transfer function places additional constraints on the controller design. The sensor is insensitive at the multiple frequencies of $1/\tau_2 \approx 30$ mHz (nulls). Also, the significant phase loss from the delay time causes noise enhancement at nulls as well as limits the gain above 30 mHz. Furthermore, some of the nulls are well located in the LISA band. This would significantly jeopardize the sensitivity of the LISA at these frequencies.

2.1.2. Dual arm locking In dual arm locking both of the two interferometry signals are used to construct the arm locking sensor. It has been demonstrated that the information on the second arm could effectively push the first null in the sensor response beyond the LISA band. The mapping vector of dual arm locking takes the form of $[1 - \frac{E(s)}{s\Delta\tau}, 1 + \frac{E(s)}{s\Delta\tau}]$, where $\Delta\tau = (\tau_2 - \tau_3)/2$ and $E(s)$ is an additional low-pass filter to maintain the stability of the sensor for frequencies above $1/\Delta\tau$. Consequently, the sensor transfer function of dual arm locking is given by

$$\begin{aligned} H_D(s) &= \begin{bmatrix} P_{12}(s) \\ P_{13}(s) \end{bmatrix} \cdot [1 - \frac{E(s)}{s\Delta\tau}, 1 + \frac{E(s)}{s\Delta\tau}] \\ &= P_{12}(s) + P_{13}(s) - \frac{E(s)}{s\Delta\tau}(P_{12}(s) - P_{13}(s)) \\ &= P_+(s) - \frac{E(s)}{s\Delta\tau} P_-(s) \end{aligned} \tag{6}$$

where $P_+(s) = P_{12}(s) + P_{13}(s)$ and $P_-(s) = P_{12}(s) - P_{13}(s)$ are known as the common arm sensor and the differential arm sensor, respectively. The $1/s$ factor ensures that $P_-(s)$ dominates at low frequencies. The magnitude of the dual arm locking sensor is almost flat for all frequencies below $1/\Delta\tau$ and this feature allows a controller with higher gain within the LISA band.

2.2. Doppler knowledge error and the frequency pulling

The frequency of the laser beat signal depends on the known offset used at the phase-locked loop at the far spacecraft and the not so well known Doppler shift caused by the relative S/C motion. Ideally, the phasemeter demodulates the beat signal with the difference frequency of the two lasers. Consequently, the preset frequency at the phasemeter needs to be updated in real-time due to the time-variable Doppler shift, which is unfortunately difficult to estimate at a very accurate level. It appears to be possible to limit the Doppler estimation error to ~ 20 Hz per 200 s averaging time [6] by introducing additional functionality in on-board data processing.

The remaining offset will be integrated up in the arm locking controller, which causes a frequency pulling in the stabilized laser frequency. Generally a linear drift in frequency is mostly

harmless in the data post-processing. However, a large frequency drift introduces additional requirements on the tunability of the arm locked laser and consequently on that of all six lasers in the LISA constellation. In the following sections we will quantify the frequency pulling induced by Doppler errors by investigating the frequency response of a generic arm locking loop.

2.2.1. Single arm locking Figure 2 shows a generic single arm locking loop with a Doppler error input in the Laplace domain. The transfer functions of the single arm locking sensor and controller are $G(s)$ and $H(s)$, respectively. For single arm locking, the Doppler error is introduced in the demodulation at the phasemeter right before the controller. In this diagram, the closed-loop transfer function from the Doppler error input to the stabilized laser noise output is given by

$$TF_{\mathrm{D}}(s) = \frac{G(s)}{1 + H(s)G(s)}. \tag{7}$$

In a standard control loop when the controller yields the high gain limit $G(s) \to \infty$, the transfer function is reduced to

$$TF_{\mathrm{D}}(s) \approx \frac{1}{H_1(s)} \approx \frac{1}{\tau s} \qquad \text{(at low frequencies)}. \tag{8}$$

The frequency response of a DC-coupled single arm locking loop is equivalent to an integrator, which accumulates the Doppler error over time and causes a drift in the output frequency. In the time domain, the instantaneous output frequency is given by the convolution between the instantaneous Doppler error input and the transfer function described above. Over short time intervals the Doppler error is constant and the laser frequency changes by

$$\begin{aligned} \Delta\omega_{\mathrm{L}}(t) &= \frac{1}{\tau}\int \Delta\omega_{\mathrm{D}}\mathrm{dt} \\ &= \frac{\Delta\omega_{\mathrm{D}}}{\tau}t \end{aligned} \tag{9}$$

One potential solution is to reduce the controller gain gradually at low frequencies. This is known as AC-coupling. In the low gain limit, we then have

$$TF_{\mathrm{D}}(s) \approx G(s) \ll 1 \qquad \text{(at low frequencies)}. \tag{10}$$

In the low gain limit, the laser frequency changes simply by the Doppler error multiplied with the low controller gain. Thus, in the presence of an AC-coupled controller the Doppler error will not be accumulated by the controller and consequently the residual effect is no more than an insignificant offset added to the output laser frequency.

2.2.2. Dual arm locking In dual arm locking the two arms generate two independent Doppler errors. These can be combined to construct a common and a differential Doppler error which will show up in the common and differential arm sensors and will be amplified by the arm locking gain:

$$TF_{\mathrm{D}+}(s) = \frac{G(s)}{1 + H_{\mathrm{D}}(s)G(s)} \tag{11}$$

$$TF_{\mathrm{D}-}(s) = \frac{G(s)E(s)}{\Delta\tau s[1 + H_{\mathrm{D}}(s)G(s)]}, \tag{12}$$

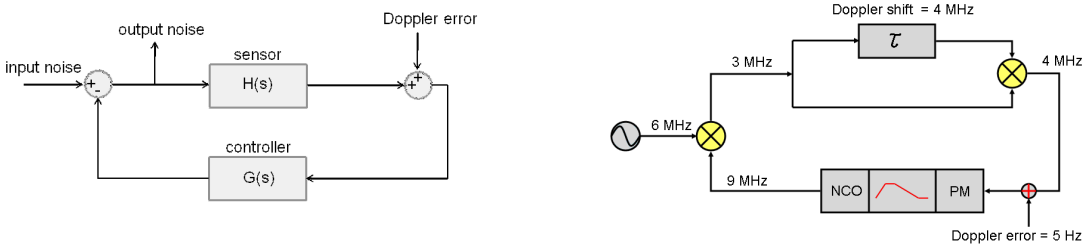

Figure 2. Left: A generic single arm locking loop with a Doppler error input in the Laplace domain. The Doppler error is introduced in the demodulation at the phasemeter. We define the (effective) sensor $H(s)$ to be the components before the Doppler error point and the (effective) controller $G(s)$ to be the components after the Doppler error point. Right: The experimental configuration of single arm locking in the presence of a Doppler error of 5 Hz. An input free-running VCO signal is demodulated by a tracking NCO signal. The output of the mixer is sent to a single arm locking sensor and shifted by a Doppler frequency. The controller filter (represented by the red curve) is AC-coupled in order to remove the frequency pulling effect from the Doppler error.

In the high gain limit Equation (10) is approximately equal to $1/H_{\rm D}(s)$. Since the magnitude of the dual arm locking sensor is flat at low frequencies, a common Doppler error will only cause a frequency offset in dual arm locking.[1]

In the differential arm, we have $E(s) \approx 1$ and $H_{\rm D}(s) \approx 2$ at low frequencies and in the high gain limit the equation approaches $1/2\Delta\tau s$. This frequency response corresponds to a frequency drift rate of $\Delta\omega_{\rm D-}/2\Delta\tau$. Several kinds of approaches have been proposed to reduce this frequency pulling. Some of them will be discussed in more detail in Section 4.

3. Single arm locking experiments in the presence of a Doppler error

The feasibility of single arm locking has been studied experimentally by several highly idealized verification experiments. All of these benchtop experiments simulated an ideal situation without any Doppler shift [8, 9] or when the Doppler frequency was perfectly accounted for at the phasemeter [3, 10]. This is unrealistic and the difference between the real and the estimated Doppler frequency will generate a Doppler error which will cause the above discussed laser frequency pulling effect. The Doppler frequency can be estimated using various techniques. For example laser ranging will also measure the relative velocity between the spacecraft or the averaged laser beat frequency allows to estimate the Doppler frequency directly. The performance of these techniques depends on many factors such as the initial laser frequency noise, integration time, differential clock noise, or the ability to exchange data between the S/C. Expected Doppler errors also depend on the functionality installed in the phasemeter and range from a few Hz to a few kHz [6]. In this section we will discuss a pioneering experiment in which a constant Doppler error is introduced into our single arm locking loop and a designed AC-coupled controller is dedicated to eliminate the frequency pulling.

In our preliminary experiment we use a single arm locking loop featuring the EPD unit to stabilize the frequency of a numerical control oscillator (NCO) to a noisy voltage controlled oscillator (VCO). Figure 2 illustrates the experimental configuration, in which a 6 MHz free

[1] This characteristics is to be distinguished from the frequency response of a common arm locking loop to a common Doppler error. In that case the arm locking sensor is replaced with $H_+(s) = P_+(s)$. Consequently, in the high gain limit a common Doppler error $\Delta\omega_{\rm D+} = \Delta\omega_{\rm D1} + \Delta\omega_{\rm D2}$ will cause the frequency pulling with a drift rate of $\Delta\omega_{\rm D+}/2\bar{\tau}$.

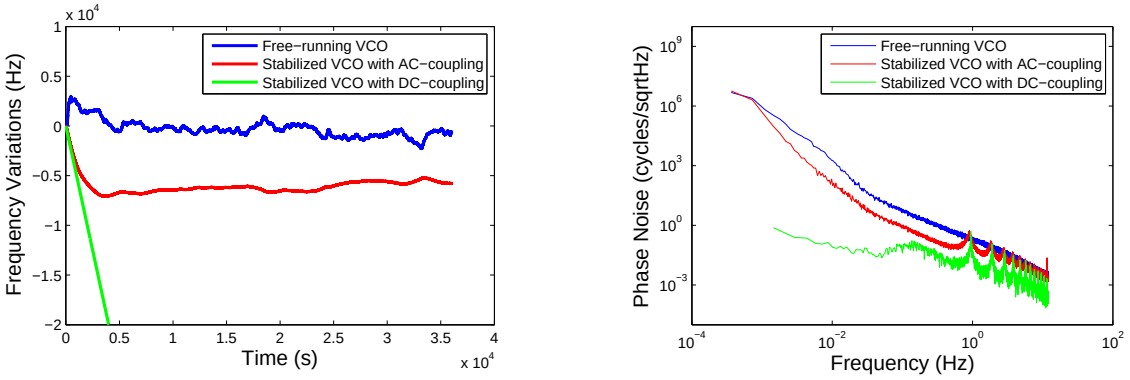

Figure 3. The measurement results of the experiment shown in Figure 2. Left: time series of a free-running VCO signal, a stabilized VCO signal with the AC-coupled controller and a stabilized VCO signal with a standard DC-coupled controller. The AC-coupled controller is capable of removing the frequency pulling that shows up in the situation with the DC-coupled controller. Right: linear spectral densities of the phase noise of the three time series. Although the Doppler error does not cause frequency pulling with the AC-coupled controller, the controller gain is significantly limited and the noise suppression performance is compromised.

running VCO signal is demodulated with a 9 MHz NCO signal. The beat signal of 3 MHz is then split into a prompt signal and a signal which is delayed by 1 s as well as shifted by 4 MHz. The delayed signal is mixed with the prompt signal. The output of this mixer is the Doppler shifted single arm locking error signal. The phasemeter will demodulate the error signal with a pre-set frequency.

Previous experiments have shown the noise suppression when the preset frequency matches the Doppler frequency perfectly. Figure 3 shows for the first time the performance of arm locking when the pre-set frequency does not match the Doppler frequency; here we used an offset of 5 Hz. The left graph shows the 10 h time series of the free running VCO-NCO beat (blue), the time series of the beat when stabilized by an AC-coupled controller (red), and the time series when stabilized by a standard DC-coupled controller (green). The right graph shows the linear spectral densities of the phase fluctuations of the three beat signals. The DC-coupled controller has the best in-band performance but the frequency is ramping down with the expected rate of 5 Hz/s. Note that we use a fairly high low unity gain frequency (UGF) compared to LISA to perform the measurement in a reasonable time. This limits the noise suppression in our experiments compared to the noise suppression expected in LISA.

4. Dual arm locking simulations

We are currently in the process of setting up a dual arm locking experiment. Here we report about time-domain simulations of dual arm locking with Doppler errors in LISA. Our time-domain simulation is running on a Matlab Simulink model with floating point arithmetic. For our simulated noise source we use the phase noise integrated from 30 Hz/$\sqrt{\text{Hz}}$ white frequency noise.

4.1. Dual arm locking with AC-coupled controller

We designed an AC-coupled controller based on the zeros and poles listed in Table 1. The other parameters used in our simulation are listed in Table 2.

The black curve in Figure 4 is the open-loop transfer function which is given by the dual arm locking sensor (the blue curve) multiplied by the AC-coupled controller (the red curve) with a

Table 1. Parameters of the AC-coupled filter used in simulations

zeros (Hz)	poles (Hz)
10^{-7}	5×10^{-6}
10^{-7}	5×10^{-6}
10^{-6}	3×10^{-3}
5×10^{-5}	3×10^{-3}
5×10^{-5}	3×10^{-3}
0.1	3×10^{-3}
0.3	3×10^{-3}

Table 2. Parameters of the time-domain simulation of AC-coupled dual arm locking.

$\bar{\tau}$	$\Delta\tau$	$\Delta\omega_{\mathrm{D1}}$	$\Delta\omega_{\mathrm{D2}}$	G_0
33 s	0.255 s	2 kHz	3 kHz	100

loop gain factor G_0. The AC-coupled controller consists of a $f^{-1/2}$ slope low-pass filter for the high frequency suppression and a high pass filter to reduce the frequency pulling. The open-loop transfer function provides a bandwidth of around 42 kHz and a unity gain frequency of 15 μHz at low frequencies. The yellow curve and the cyan curve demonstrate the effective controller G_{eff} and the effective sensor H_{eff} in the differential arm respectively.

The closed-loop frequency response to the differential Doppler error is illustrated by the green curve in the figure. Depending on the gain level of the open-loop transfer function $H_{\mathrm{eff}}(s)G_{\mathrm{eff}}(s)$, the closed-loop frequency response consists of three segments in different frequency regions:

$$TF_{\mathrm{D}-}(s) = \begin{cases} \frac{1}{H_{\mathrm{eff}}(s)} \approx \frac{1}{2\Delta\tau s}, & \text{when } f \gg f_{\mathrm{UG}} \\ \frac{G_{\mathrm{eff(s)}}}{1+H_{\mathrm{eff}}(s)G_{\mathrm{eff(s)}}}, & \text{when } f \sim f_{\mathrm{UG}} \\ G_{\mathrm{eff(s)}}, & \text{when } f \ll f_{\mathrm{UG}} \end{cases} \tag{13}$$

where f_{UG} is the lower UGF of the open loop transfer function (black curve in right graph of Fig. 4).

We are more interested in the region where the closed-loop frequency response is approximately equal to the effective controller, i.e., $TF_{\mathrm{D}-}(s) = G_{\mathrm{eff(s)}} = G_0G(s)/(\Delta\tau s)$. The $1/s$ slope in the frequency response indicates a Doppler error induced pulling still occurs in the output frequency. However, compared with the large gain factor of $1/(2\Delta\tau)$ in the DC-coupling situation, the gain factor now is significantly reduced due to the low gain of the AC-coupled controller. If we recall that the gain factor of $1/s$ is directly proportional to the drift rate of the frequency pulling, it is straightforward to derive the reduced drift rate given by

$$\left(\frac{\mathrm{d}\omega_{\mathrm{L}}}{\mathrm{dt}}\right)_{\mathrm{AC-coupled}} = 2G_0G(s)\left(\frac{\mathrm{d}\omega_{\mathrm{L}}}{\mathrm{dt}}\right)_{\mathrm{DC-coupled}}. \tag{14}$$

This relation indicates that the reduced drift rate is also directly proportional to the loop gain. Our time-domain simulation is based on a long arm length mismatch of $2\Delta\tau = 0.51$ s and an inaccurate differential Doppler estimation of $\Delta\omega_{\mathrm{D}-} = 1$ kHz. Without the AC-coupling scheme

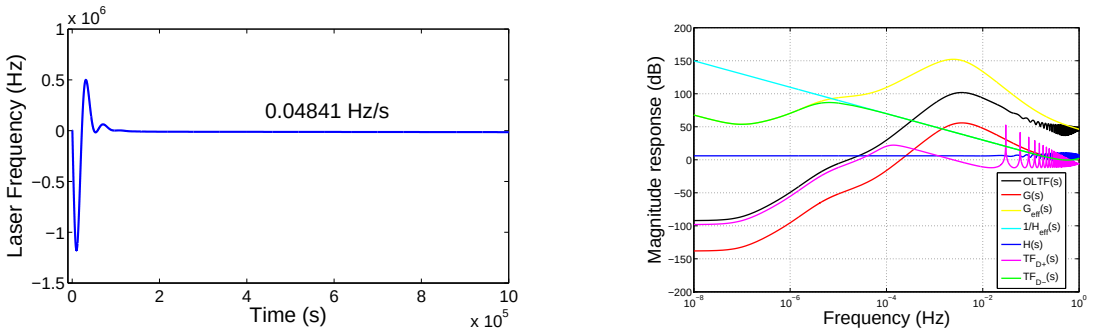

Figure 4. Left: Simulated time series of the output frequency change due to a 1 kHz differential Doppler error in a dual arm locking loop with an AC-coupled controller. The initial transients during locking acquisition also appear in the output frequency. Without the AC-coupling the drift rate would be 1961 Hz/s. Right: Modelled frequency responses of a dual arm locking loop to common and differential Doppler errors in the presence of an AC-coupled controller. Without the AC-coupled controller the frequency response to a differential Doppler error (the green curve) would follow $1/H_{\rm eff}(s)$ (the cyan curve). In the presence of the AC-coupled controller it starts to deviate when passing the unity gain frequency and the gain is consequently scaled down by the controller gain.

the drift rate would be 1 kHz/0.51 s $\approx$ 1961 Hz/s for a high gain DC-coupled controller. Figure 4 shows the time series of the variation of the laser frequency using our AC-coupled controller. The drift rate has been reduced to 0.04841 Hz/s which is exactly what we expect based on the frequency domain analysis presented above. Note that we reduced the laser frequency noise in this simulation to zero to be able to determine the drift rate with this accuracy.

4.2. Dual arm locking with modified sensor

A second option to reduce the frequency pulling effect has also been proposed by Kirk McKenzie [6]. The basic idea of the modified dual arm locking sensor is to combine the benefits of common arm locking and dual arm locking by amplifying the common arm sensor below $1/\bar{\tau}$ and keeping the dual arm sensor above $1/\bar{\tau}$. This has the additional advantages that many other technical noise sources are reduced as well.

We modified our original dual arm locking sensor based on the same principle but used a simpler approach. The common arm signal is integrated by $1/s$ and scaled by $1/\bar{\tau}$ such that the frequency response of the common arm signal dominates at frequencies below $1/\bar{\tau}$. On the other hand, the original dual arm locking sensor signal is filtered by a high-pass filter $F(s)$ designed in a manner that the combined frequency response stays well below the common arm at frequencies below $1/\bar{\tau}$ and smoothly returns to the original level. Therefore, the sensor transfer function of modified dual arm locking is given by

$$H_{\rm MD}(s) = \frac{1}{\bar{\tau}s}P_+(s) + F(s)H_{\rm D}(s) \tag{15}$$

The parameters of our simulation model are listed in Table 3 and the corresponding modified sensor transfer function is shown in Figure 5.

To analyse the frequency response of modified dual arm locking to Doppler errors, we follow the same routine by considering the common arm and differential arm independently. First, the expression of $H_{\rm MD}(s)$ allows us to rewrite the sensor transfer function in the form of a combination of common arm and differential arm, i.e.,

Table 3. Parameters of the time-domain simulation of modified dual arm locking.

$\bar{\tau}$	$\Delta\tau$	$\Delta\omega_{\mathrm{D1}}$	$\Delta\omega_{\mathrm{D2}}$	G_0
33 s	0.165 s	4 kHz	2.5 kHz	10

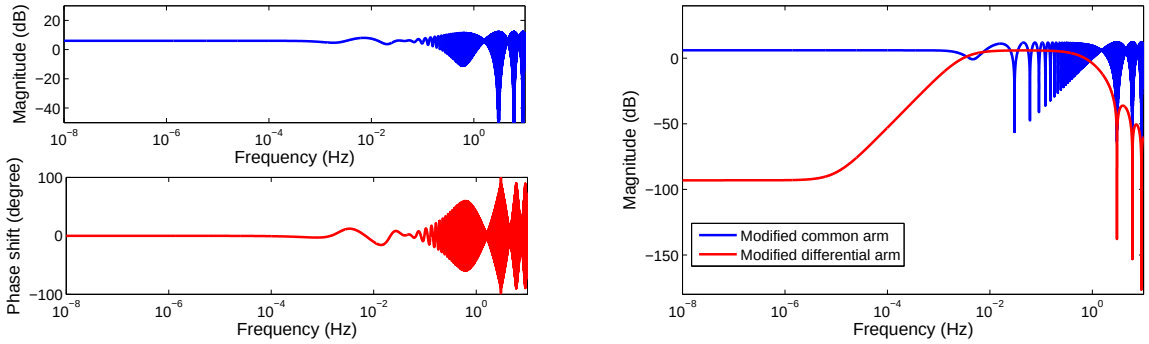

Figure 5. Left: The frequency response and phase response of our modified dual arm locking sensor. Right: Frequency responses in the common arm and differential arm of our modified sensor. Comparing to the original frequency responses, the common arm is integrated and high-pass filtered such that it dominates at frequencies below $1/\bar{\tau}$ and above $1/\Delta\tau$, while the differential arm is high-pass filtered such that the gain at frequencies below $1/\bar{\tau}$ is efficiently suppressed.

$$\begin{aligned} H_{\mathrm{MD}}(s) &= \frac{1}{\bar{\tau}s}P_+(s) + F(s)H_{\mathrm{D}}(s) \\ &= \frac{1}{\bar{\tau}s}P_+(s) + F(s)(P_+(s) - \frac{E(s)}{\Delta\tau s}P_-(s)) \\ &= (\frac{1}{\bar{\tau}s} + F(s))P_+(s) - \frac{E(s)F(s)}{\Delta\tau s}P_-(s) \end{aligned} \tag{16}$$

Consequently, the effective common arm sensor and effective common arm controller are given by

$$H_{+\mathrm{eff}}(s) = P_+(s) \tag{17}$$

$$G_{+\mathrm{eff}}(s) = G_0(\frac{1}{\bar{\tau}s} + F(s))G(s). \tag{18}$$

The effective differential arm sensor and effective differential arm controller are given by

$$H_{-\mathrm{eff}}(s) = P_-(s) \tag{19}$$

$$G_{-\mathrm{eff}}(s) = \frac{G_0E(s)F(s)G(s)}{\Delta\tau s}. \tag{20}$$

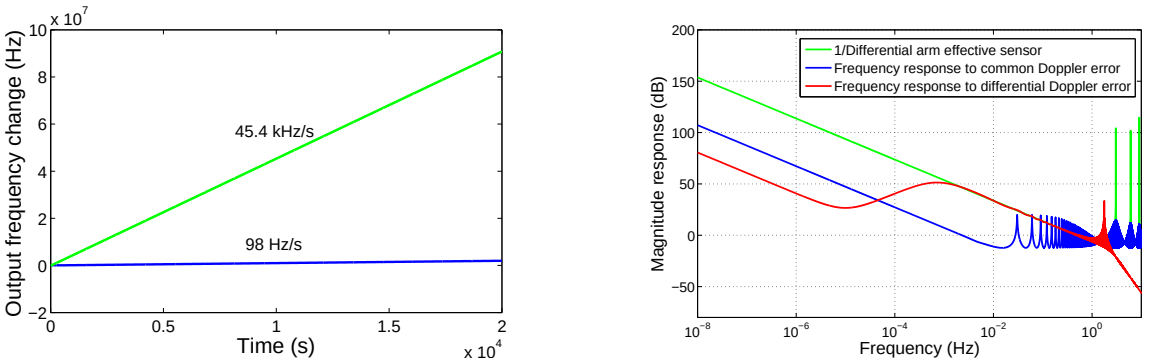

Figure 6. Left: Simulated time series of the output frequency change due to a 6.5 kHz common Doppler error and a 1.5 kHz differential Doppler error in a dual arm locking loop with a modified dual arm locking sensor. The modified sensor is capable of reducing the frequency drift rate to the level of common arm locking (6.5 kHz/(2 × 33 s) ≈ 98 Hz/s). Without the modified sensor the drift rate would be 45.4 kHz/s due to the differential Doppler error. Right: Modelled frequency responses to common and differential Doppler errors in the modified dual arm locking loop. Without the modified sensor the frequency response to a differential Doppler error would follow $1/H_{-\mathrm{eff}}(s)$ (the green curve). Due to the high-pass filter implemented in the modified sensor the gain of the differential arm is gradually suppressed lower than the gain of the common arm for frequencies below $1/\bar{\tau}$.

Substitute the relations into Equation (6) and we are able to derive the closed-loop frequency response for both paths. If we only consider the high gain limit, the frequency response to the common arm Doppler error is now

$$TF_{\mathrm{D}+}(s) \approx \frac{1}{P_+(s)} \approx \frac{1}{2\bar{\tau}s} \qquad \text{(at low frequencies)}. \tag{21}$$

This frequency response is the same as the case for common arm locking, corresponding to a frequency drift rate of $\Delta\omega_{\mathrm{D}+}/2\bar{\tau}$. The frequency response to the differential arm Doppler error takes the form

$$TF_{\mathrm{D}-}(s) = \frac{\frac{G_0E(s)F(s)G(s)}{\Delta\tau s}}{1 + P_-(s)\cdot\frac{G_0E(s)F(s)G(s)}{\Delta\tau s}}. \tag{22}$$

At low frequencies we have $E(s) \approx 1$ and $P_-(s) \approx 2\Delta\tau s$, therefore the above equation is simplified into

$$TF_{\mathrm{D}-}(s) = \frac{1}{\Delta\tau s}\cdot\frac{G_0F(s)G(s)}{1 + 2G_0F(s)G(s)} \tag{23}$$

The transfer function will be reduced significantly if the magnitude of $F(s)$ falls fast enough towards lower frequencies to overcome the gains of G_0 and $G(s)$. In this case the drift rate of the lasers scales with $1/(2\bar{\tau})$ rather than $1/(2\Delta\tau)$.

The frequency responses of both common and differential arms are plotted in Figure 6. In this modified dual arm locking model the common arm Doppler error dominates over the differential Doppler error. For our case the Doppler error in each arm was 4 kHz and 2.5 kHz, respectively. Based on the calculation above the reduced frequency drift rate should be 6.5 kHz/(2 · 33 s) = 98.5 Hz/s. The simulated time series is shown in Figure 6, featuring a reduced drift rate of 98 Hz/s while the original drift rate due to the differential Doppler error would be 45.4 kHz/s.

5. Conclusions

We discussed the impact of the relative SC motion and the induced Doppler shifts on arm locking. We discussed how the Doppler offset produces a ramp in the laser frequency in a standard 'high gain at low frequencies' controller. We also showed how this ramp depends on the final sensor design. This paper also presents the first ever experimental proof of arm locking in a realistic, non-static LISA configuration. We developed an AC-coupled controller which significantly reduces the induced ramp in the laser frequency. In addition to the single arm locking experiments, we also present detailed simulation results for the dual arm locking and modified dual arm locking sensor with Doppler offsets. The numerical results confirm the theoretically expected changes in the laser frequency and show that the modified dual arm locking sensor will also limit the changes in the laser frequency. This work was supported by NASA grant 07-ATFP07-0116.

References

[1] LISA science requirement document version 3.0 2005 http://www.srl.caltech.edu/lisa/documents/SRD_v3_0_sb.pdf 1

[2] Sheard B, Gray M, McClelland D and Shaddock D 2003 Laser frequency stabilization by locking to a LISA arm *Phys. Lett.* A **320** 9-21 1

[3] Wand V, Yu Y, Mitryk S, Sweeney D, Preston A, Tanner D, Mueller G, Thorpe J I and Livas J 2009 Implementation of armlocking with a delay of 1 second in the presence of Doppler shifts *J. Phys.: Conf. Series* **154** 012024 1, 5

[4] Thorpe J I, Cruz R J, Sankar S R, Mueller G and McNamara P 2004 First step toward a benchtop model of the Laser Interferometer Space Antenna *Opt. Lett.* **29** 2843-45 1

[5] Thorpe J I, Cruz R J, Sankar S and Mueller G 2005 Electronic phase delay: A first step towards a bench-top model of LISA *Class. Quantum Grav.* **22** S227-34 1

[6] McKenzie K, Spero R E, Shaddock D A 2009 The performance of arm locking in LISA arXiv:0908.0290v2 [gr-qc] 3, 5, 8

[7] Sutton A and Shaddock D A 2008 Laser frequency stabilization by dual arm locking for LISA *Phys. Rev.* D **78** 082001 3

[8] Marin A *et al* 2005 Phase locking to a LISA arm: First results on a hardware model *Class. Quantum Grav.* **22** S235-42 5

[9] Thorpe J I and Mueller G 2005 Experimental verification of arm-locking for LISA using electronic phase delay *Phys. Lett.* A **342** 199-204 5

[10] Livas J C, Thorpe J I, Numata K, Mitryk S, Mueller G and Wand V 2009 Frequency-tunable pre-stabilized lasers for LISA via sideband locking *Class. Quantum Grav.* **26** 094016 5